LAGRANGIAN AND EULERIAN DESCRIPTION OF TURBULENCE IN THE UNSTABLE ATMOSPHERIC BOUNDARY LAYER

Giorgio Querzoli

Finito di stampare nel mese di Gennaio 1995
dalla Lit. N. Libero, per conto della CUEN

LAGRANGIAN AND EULERIAN DESCRIPTION OF TURBULENCE IN THE UNSTABLE ATMOSPHERIC BOUNDARY LAYER

Giorgio Querzoli

Dipartimento di Meccanica e Aeronautica
Università di Roma "La Sapienza" - Via Eudossiana, 18 - 00184 Roma

Summary

The convection in the atmospheric boundary layer are investigated by means of a laboratory model. Two optical, non-intrusive techniques are used to measure the velocity field: the Laser-Doppler Velocimetry and Particle Tracking Velocimetry. The former describes the field in terms of time history of the velocity at fixed locations, which means it gives an Eulerian description of the field; from these measurements, the second-order moments, probability distributions, and autocorrelations of the velocity fluctuations are evaluated. Together with the vertical velocity, the temperature has also been probed by a thermocouple to determine the turbulent kinematic heat flux. These data are compared with atmospheric experiments, and they are in good agreement. This means that the laboratory model accurately simulates the atmospheric phenomena. The Eulerian integral time scales are also evaluated from the autocorrelations.

The second technique, Particle Tracking Velocimetry, is based on tracking non-buoyant particles, uniformly dispersed within the working fluid, by means of the image analysis. This technique describes the turbulence in terms of variability of the velocity along particle trajectories, which means it furnishes a Lagrangian description. The Lagrangian autocorrelations are presented with the vertical variability of the Lagrangian integral time scales. Though the Eulerian time scales are seen to be nearly constant in the bulk of the layer, the Lagrangian ones exhibit large changes with height. Thus a single value, representative of the whole layer has not been found.

The basic phenomena driving the convective mixing of the atmosphere are the hot updrafts and cold downdrafts. They are outlined separately by means of the conditional sampling.

Trajectories acquired by the Particle Tracking Velocimetry have been parted into two sets: the one is the set of trajectories whose first vertical velocity is positive, the other includes trajectories whose first vertical velocity component is negative. For the two sets the autocorrelations and integral time scales are presented and compared. The behaviour of updrafts and downdrafts seems to be very different because of the presence of the top and bottom boundaries.

1. Introduction

Most of phenomena related to the quality of the air occur in the lower part of the atmosphere, in the region affected by the earth surface that is called Atmospheric Boundary Layer. As a matter of fact, the Atmospheric Boundary Layer is the region where nearly all the pollutants are released and where the prediction of their concentration is of great interest because it concerns the public health.
A detailed fluid-dynamical description of the Atmospheric Boundary Layer is the key point of the management of the environmental resources to successfully control the air quality. The description of the turbulence is useful for the interpretation of the data collected by monitoring nets. It is also important for the understanding of the physical phenomena governing the pollutant dispersion in order to develop numerical models for the prediction of the effects on the environment (Baerentsen and Berkowicz 1984). Most of the investigations of the Atmospheric Boundary Layer have been carried out by means of field experiments (Coulman 1978, Kaimal et al. 1976, Lenschow 1974, Lenschow et al. 1980, Hildebrand and Ackerman 1984, Young 1988b,c,d). Measurements were taken using instrumented airplanes, flying along straight paths at fixed heights. They recorded velocity, temperature, moisture and other quantities useful for the description of the atmosphere. Recently a new class of instruments, based on the remote sensing, have been developed. They give vertical profiles of velocity (SODAR), pollutant concentration (LIDAR) and temperature (RASS) (Stull 1988). Nevertheless, the main drawback of the field experiments is that the boundary conditions are not a priori determinable. As a consequence, the measurements can be performed only in the days in which the meteorological conditions meet the requirements of experiment. Moreover, due to the large scale phenomena, and to the daily cycle, the phenomena cannot be assumed steady for a long time, so the amount of the acquirable data is limited. Anyway, there are some conditions, such as the Unstable Boundary Layer (UBL), that are well simulated by means of laboratory models. This means, that one can run the experiment, with the same boundary and initial conditions, as many times as is needed to achieve a reliable statistical base.
The Unstable Boundary Layer is the region of the atmosphere where strong convective mixing occurs, due to the heat flux from the heart surface associated with the solar radiation. It includes the first thousands of meters, when the mean wind is weak and the sky is clear, as the mechanical production of turbulence kinetic energy (due to the shear) is negligible in comparison with the buoyant production. The UBL grows since the sunrise, through a penetrative convection into a stable layer called Capping Inversion, in which the potential temperature increase with height (Young 1988a, Wyngaard 1985). Since the UBL is usually bounded on

the top by the Capping Inversion, all the pollutants released within the UBL are trapped and cannot spread into in the upper atmosphere. Thus they are found in high concentrations in the proximity of the soil. This is the reason for the interest in predicting the pollutant dispersion from sources placed within the UBL (Willis and Deardorff 1976).
For the investigation of the UBL, a laboratory model has been used. It consists of a convection chamber filled with water, in which the thermal stratification of the atmosphere was reproduced. The lower surface was heated in order to simulate the solar radiation of the soil. The velocity was investigated both from the Eulerian and Lagrangian point of view. In the former, the time history of the velocity is given at fixed locations in the vertical centreline of the tank, by means of the Laser-Doppler Velocimetry (LDV). This is a non-intrusive technique and non-sensitive to the temperature fluctuations of the working fluid. In the Lagrangian description, on the other hand, the time histories of the velocity are given along the trajectory of each fluid particle during its motion within the field. The particles are identified by means of their position at a reference time. Such a description was obtained by the Particle Tracking Velocimetry (PTV), that is a technique based on the tracking of non-buoyant particles, uniformly dispersed in the working fluid. Series of images are taken at constant time intervals by a video-camera and recorded. Then the images are analysed in order to identify the trajectory of each particle, and the velocities are computed.
From the description of the velocity field, it is possible to evaluate the Lagrangian statistics, such as the integral time scale, that are usually estimated from Eulerian measurements. The use of the laboratory model allowed to achieve a detailed description of how these quantities change with height. In the fields experiments, only a single value of the statistics was evaluated for the whole UBL, due to the big practical difficulties in performing Lagrangian measurement in atmosphere. Moreover, the data-set was conditionally sampled in order to selectively describe two phenomaena that play a fundamental role in the convective mixing of the UBL: the hot, uprising thermals and the cold, downdrafts.

2. Similarity

The comparison of data collected in field experiments with data obtained in laboratory relies on the similarity proposed by Deardorff (1970). The basic assumption of such a similarity is that phenomena occurring in the UBL depend only on three parameters:
z_i: height of the UBL,
q_s: surface kinematic heat flux,
$\alpha \cdot g$: buoyancy parameter,
where α is the thermal expansivity and g the acceleration of gravity. Through these parameters, the scaling quantities are obtained by means of the dimensional analysis:

convective velocity $w_* = \sqrt[3]{g \cdot \alpha \cdot q_s \cdot z_i}$,

convective temperature $\vartheta_* = \frac{q_s}{w_*}$,

convective time $t_* = \frac{z_i}{w_*}$.

Universal vertical profiles, that are non-dependent on the particular conditions of each experiment can be obtained by plotting the UBL statistics in non-dimensional form by means of the above mentioned parameters. Typical values of these parameters both in atmosphere and in the tank are reported in Table 1.

Table 1

Typical values of scaling parameter	Tank	Atmosphere
z_i	$0.10\,m$	$200 \div 2{,}000\,m$
q_s	$0.4 \cdot 10^{-3}\,m\,K\,s^{-1}$	$0.2m\,K\,s^{-1}$
w_*	$0.004m\,s^{-1}$	$1 \div 2\,m\,s^{-1}$
t_*	$15\,s$	$1200\,s$
θ_*	$0.1\,K$	$0.1\,K$

The similarity is valid if the mechanical production of turbulence kinetic energy is negligible with respect to the buoyant production. Let L indicate the Monin-Obukhov length:

$$L = \frac{-\overline{\vartheta} \cdot u_*^3}{g \cdot q_s \cdot k}, \tag{1}$$

where u_* is the friction velocity, k the thermal conductivity, and $\overline{\vartheta}$ the mean temperature of the UBL. Let U indicate the mean wind, the above constrain can be written as (Willis and Deardorff 1976):

$$U < 6 \cdot w_* \tag{2}$$

$$-\frac{z_i}{L} >> 1 \tag{3}$$

In the proximity of the ground there is a layer in which the mechanical production of turbulent kinetic energy is predominant (Surface Layer), due to the presence of the surface, therefore the similarity hold only for $-z/L > 1$.
In general, the UBL evolves in time, nevertheless it is possible to assume a state of moving equilibrium during its evolution, i.e. even if the scaling parameters are changing, the system

can be considered to evolve through a succession of steady states (quasi-steadiness hypothesis). This assumption is thought to be valid if the turbulence time scale (order of t_*) is much less than the time scale of the changing boundary conditions (Wyngaard 1985). Through the use of this similarity the laboratory model was validated by comparing the observed statistics with those measured in atmosphere.

3. Experimental set-up

The laboratory model is a tank whose horizontal dimensions are 41.0 *cm* x 41.0 *cm*. The working fluid is water. At the top of the water a 3 *cm* thick styrene slab floats to insulate the upper boundary. The side-walls are of glass, 0.8 *cm* thick, whereas the tank lower surface is a 0.8 *cm* thick aluminium plate. In contact with the underside of the plate is a heat exchanger consisting of a 2.5 *cm* deep chamber filled with water. Immersed in the water is a copper spiral shaped channel, 0.9 *cm* in diameter, in which the heating water flows at 1.5 *l/s* rate. The path of the channel is designed to minimise horizontal temperature gradients along the tank lower boundary. The temperature of the water flowing in the spiral is kept constant by a precision heather with a 0.1°C tolerance. The upward heat flux at the lower surface approximate the heating of a uniform terrain due to the solar radiation.
During each experiment, the tank was filled to a depth of 10.0 *cm* with degassed water at ambient temperature. The overlaying Capping Inversion was then generated by slowly floating a 10.0 *cm* deep layer of warmer water (at temperature 20°C higher than ambient one). After about half an hour the heating was applied to the lower surface. This is a time sufficient for the disturbances introduced during the filling to be damped and to produce a nearly constant vertical temperature gradient by molecular diffusion between 7.0 *cm* and 13.0 *cm* height. A period of 240 *s* was then left for the turbulent convection to fully develop before starting the measurements.
The law of growth of the UBL was estimated, in a preliminar series of experiments, considering vertical temperature profiles at constant time intervals (Figure 1). The temperature acquired in the tank can be assumed equivalent to the potential temperature in atmosphere since the transformations of fluid particles in the tank are essentially adiabatic. The profiles were probed by a thermocouple (0.05 *cm* in diameter) traversing the depth of the tank along the centreline. The height of UBL, z_i, was evaluated by individuating the height at which the temperature gradient suddenly reaches large positive values.

4. Experimental procedure

Two series of experiments with the same boundary and initial conditions were performed to determine the vertical profiles of the turbulence characteristics. During each run, the acquisition begun 240 *s* after the heating had been applied, and lasted for 1000 *s*. In the first series the Laser-Doppler Velocimetry was used in order to describe the velocity field from the

Eulerian point of view whereas, in the second series a Lagrangian description was achieved through the use of the Particle Tracking Velocimetry. The experimental set-up for the two cases are outlined below.

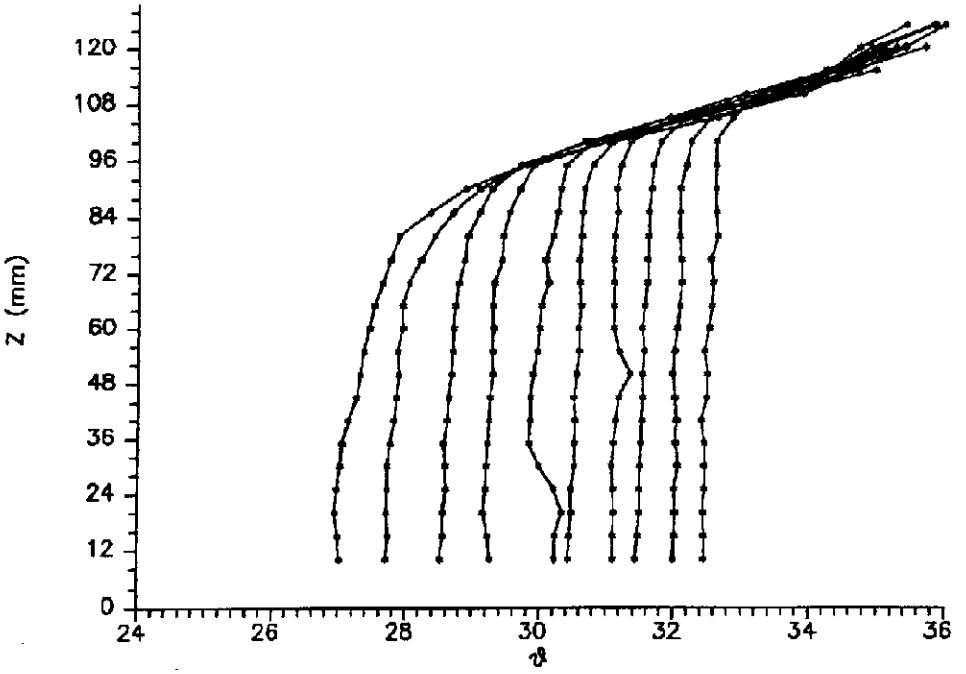

Fig. 1 - 10 Vertical profiles of temperature acquired at 100 s intervals. The first profile corresponds to 240 s after the heating is applied. It can be noticed the Capping Inversion in which the temperature gradient is almost constant.

4.1 Laser-Doppler Velocimetry

Time histories of the vertical component of the velocity and temperature were acquired at the same location of the field. The location was kept fixed for all the acquisition period long. Experiments were then repeated measuring at the same locations the horizontal velocity component. The measuring points were in the centreline of the tank, from 1.0 *cm* to 10.0 *cm* in height. At each height, the experiment was run at least 5 times per velocity component probed, in order to have an ensemble average not dependent on the individual realisations.
Temperature was acquired at 50 *Hz* sampling rate by a thermocouple and digitised with an accuracy of 0.04°*C*.
Velocities observed in the tank were typically of order 1 *cm/s* in magnitude and fluctuated around the zero. These were severe conditions for measurement taken by LDV. Hence careful optimisation of the system was needed to achieve a good signal quality. The light source was

a 10 *mW* He-Ne Laser emitting at a wave length of 632.8 *nm*. The beam was splited in two and shifted in frequency by two Bragg cells. The first cell shifted one beam of 40.0000 *MHz*, while the second cell shifted the other beam of 39.9950 *MHz* so that a 5.0 *kHz* shift resulted for the velocity orientation detection. Hence an electronic mixer was not needed to subtract the 40 *MHz* from the photomultiplier signal with an undesirable introduction of noise. The seeding was TiO_2 particles, 220 *nm* in diameter. The output photomultiplier signal was processed by an IFA 550 (Jenson 1988) and the data acquired at random time intervals at a mean data rate of about 300*Hz* were resampled with the sample-and-hold method at 50 *Hz*.

4.2 Particle Tracking Velocimetry (PTV)

The PTV is based on the reconstruction of trajectories of non-buoyant particles, uniformly dispersed within the working fluid, through the use of the image analysis. From the information about the displacements, the velocities are computed along the particle trajectories. Hence the velocity field is naturally described from the Lagrangian point of view.

The first step of the measuring process was the image recording. The fluid (water) was seeded by styrene particles, 200 μm in diameter with density equal to that of water, and an arc lamp (1000 *W*) illuminated the tank with a beam parallel to the lower surface. Orthogonal to the light beam was a CCD video-camera connected to a video-recorder. The resulting measuring volume was the portion of the illuminated volume framed by the video-camera; it was 10.0 cm high, 12.5 *cm* wide and 5.0 *cm* deep (Figure 2). An animation controller, acting as an interface between the video-recorder and a personal computer, inserted a frame code on each image to individually recognise them during the successive analysis. The rate of image acquisition was 25 *Hz*.

The second step, consisting of the image analysis itself, was performed off-line. The entire process was driven by a personal computer connected to the recorder and to a frame-grabber. One image every 10 was digitised by the frame grabber and analysed in order to individuate the seeding particles locations (Figure 3). Then, the list of particle locations was considered to recognise the displacement of each particle from one frame to the next (Figure 4). Once displacements had been known, velocities were computed simply by dividing them by the time interval between two consecutive images.

The criteria used for the trajectory recognition are:

a) the displacement between to sequential location of a particle must be less than a given parameter D;
b) the difference between two sequential displacements of a particle must be less than a given parameter e.

The choice of the parameter D corresponds to assume a maximum velocity for the investigated field, whereas the choice of the parameter e is equivalent to assume a maximum acceleration. The tuning of these is the basic point of the PTV: if the parameters are too restrictive, high velocity trajectories are rejected whereas, if it is too large, a significant number of errors occurs during the recognition.

Fig. 2 - A multi-exposed image of the investigated field. The particles are artificially coloured to indicate the time evolution of the particle position.

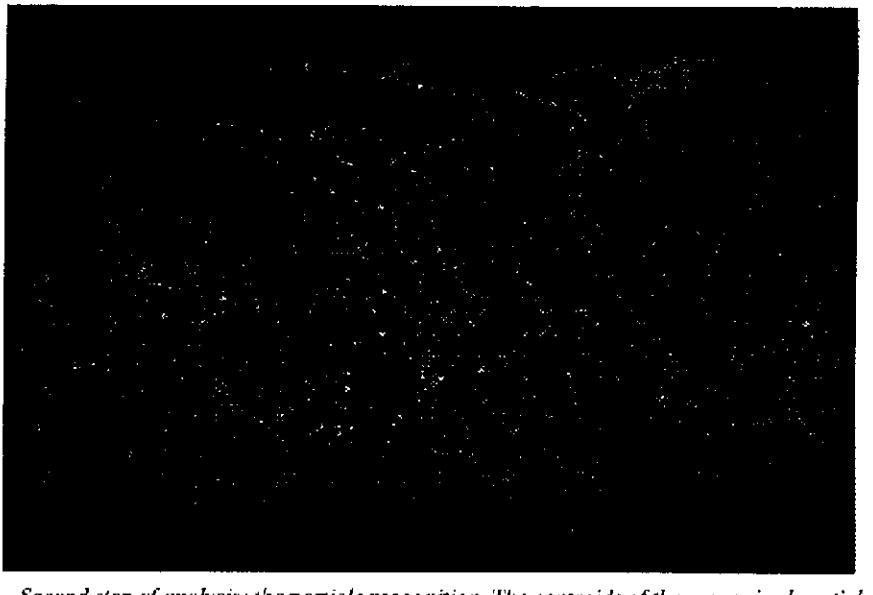

Fig. 3 - Second step of analysis: the particle recognition. The centroids of the recognised particles are indicated by a blue cross.

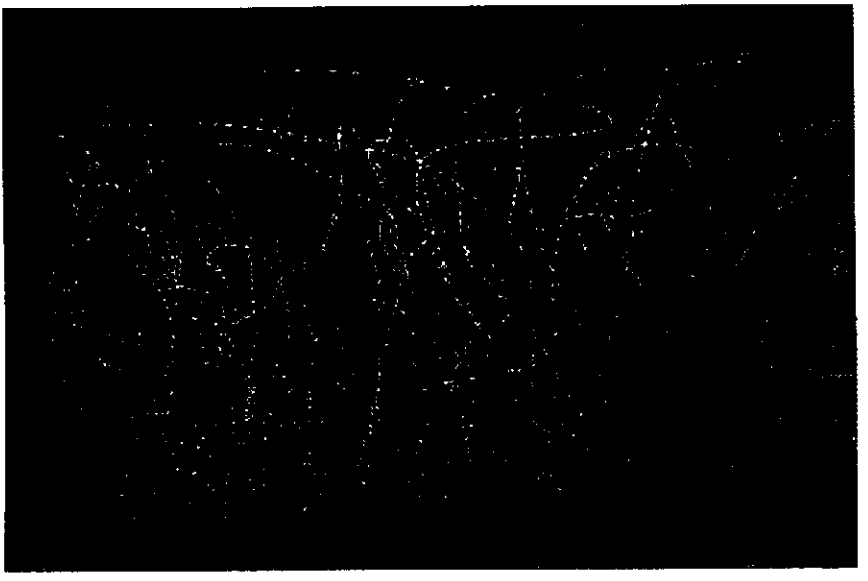

Fig. 4 - Third step of Particle Tracking Velocimetry: Trajectory recognition. red lines indicates particle trajectories.

5. Results

The results of the two series of experiment runs are presented. The Eulerian statistics are compared with atmospheric ones to validate the laboratory model, whereas no comparison was possible for the Lagrangian statistics as no suitable fields experiments have been carried out in atmosphere.

5.1 Turbulent kinetic heat flux

The non-dimensional vertical profile of the turbulent kinematic heat flux, is shown in Figure 5. The heat flux is:

$$q = \overline{w'\vartheta'} = \frac{1}{T}\int_T \left(w(t) - \overline{w}(t) \right) \cdot \left(\vartheta(t) - \overline{\vartheta}(t) \right) dt \qquad (4)$$

where T is the acquisition period, $\overline{w}(t)$ is actually zero because no subsidence is present, and the moving average temperature of the UBL $\overline{\vartheta}(t)$ is obtained from a cubic regression of the time history acquired by the thermocouple (Lumley and Panofsky 1964), assuming the temperature is uniform all over the layer.

The heat flux is normalised by the surface heat flux q_s. To achieve a suitable formulation of q_s, the heat budget equation is written under the assumption of horizontal homogeneity, no subsidence (null average vertical velocity), and neglecting latent heat and molecular conduction:

$$\frac{\partial \vartheta}{\partial t} + \frac{\partial \left(\overline{w' \vartheta'} \right)}{\partial z} = 0 \tag{5}$$

The integration of (5) from the lower surface to the height, $z_0 = k\, z_i$, at which the turbulent heat flux vanishes gives:

$$q_s = k \cdot z_i \cdot \frac{\partial \vartheta}{\partial t} \tag{6}$$

The ratio k between z_i and the height at which heat flux vanishes, was experimentally found to be 0.7. The law of growth of the UBL height had been found from temperature profiles, as mentioned above, and the mean potential temperature is known from the moving average of the thermocouple signal time history as temperature is uniform all over the height of the UBL.

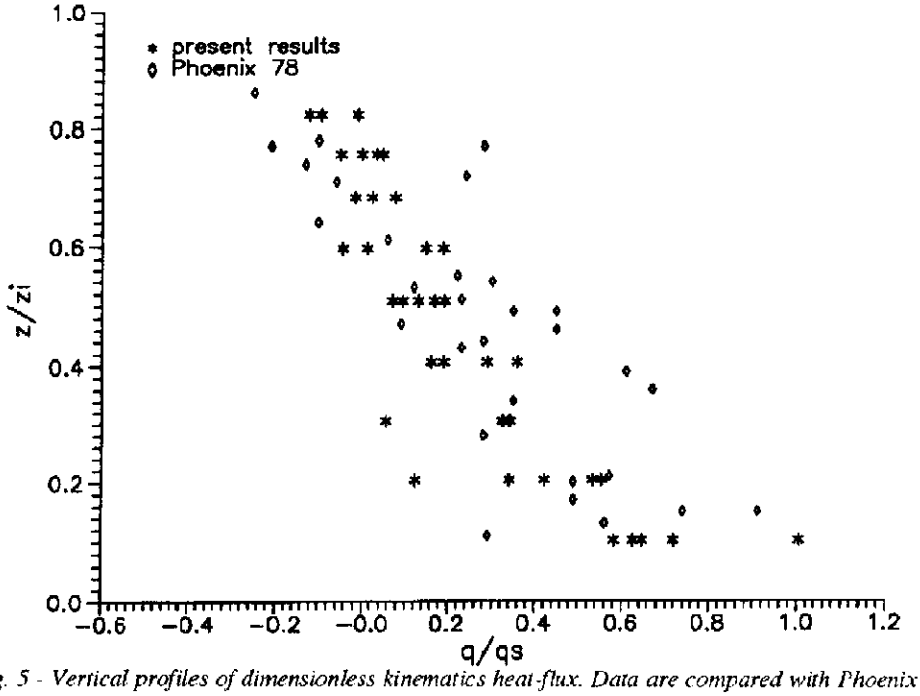

Fig. 5 - Vertical profiles of dimensionless kinematics heat-flux. Data are compared with Phoenix 78 field experiment (Young 1988b).

The non-dimensional heat flux decrease linearly with height, according to the similarity of temperature profiles as can be observed in Figure 1. Present results are compared with data from atmospheric experiment Phoenix78 (Young 1988b). A good overall agreement is apparent, though laboratory results are less scattered, presumably because they are averaged on a time much longer than the time scale of the characteristic phenomena of UBL.

5.2 Temperature variance

The temperature variance $\overline{\vartheta'^2}$, relative to ϑ_*^2 , is shown in Figure 6. The variance is seen to be large at the upper and lower boundary while it reaches a minimum at about $z/z_i = 0.6$. At the lower surface, the temperature fluctuations are large since they are forced by the heating of the surface. At the top of the UBL, the large fluctuations are due to the overlaying Capping Inversion, where strong vertical temperature gradients are observed. The present values agree quite well with the field experiment data in the lower half of the UBL, though in the upper part it is known that temperature variance is influenced by the Capping Inversion structure (Willis and Deardorff 1974).

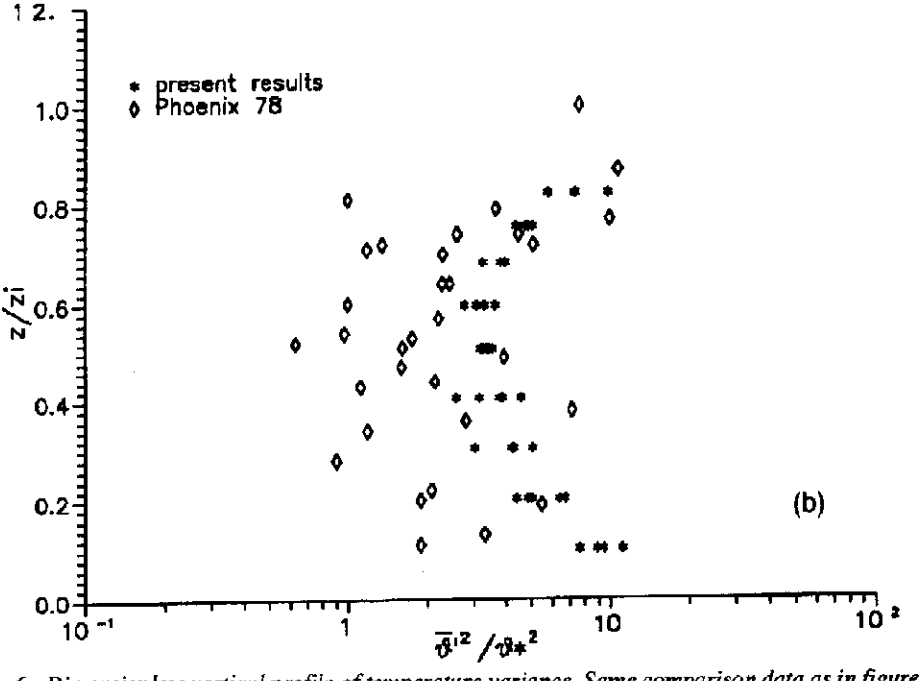

Fig. 6 - Dimensionless vertical profile of temperature variance. Same comparison data as in figure 5.

5.3 Velocity variances

The variance of non-dimensional vertical velocity is shown in Figure 7 and compared with Phoenix78 experiment (Young 1988b). It is small near the surface, due to the presence of a solid horizontal surface, where the vertical velocity component must be null. From that level, it increases up to $z/z_i = 0.3$, where it reaches a maximum, then it decreases again towards the top of the UBL, where the thermal stability damps the vertical motions. The present values show an overall agreement with the comparison data.

In Figure 8, the non-dimensional profile of the horizontal velocity variance is shown. The variance is low in the Capping Inversion and increases both at $z/z_i = 0.8$ and $z/z_i = 0.1$, while its amplitude decreases in the centre of the UBL. The large values in the proximity of the upper and lower boundaries are due to horizontal predominant motion observed at those levels. The diminished values of the present results, with respect to the atmospheric ones (Lenschow 1968, 1970), depend on the effect of the side-walls that cut off the large horizontal structures present in atmosphere.

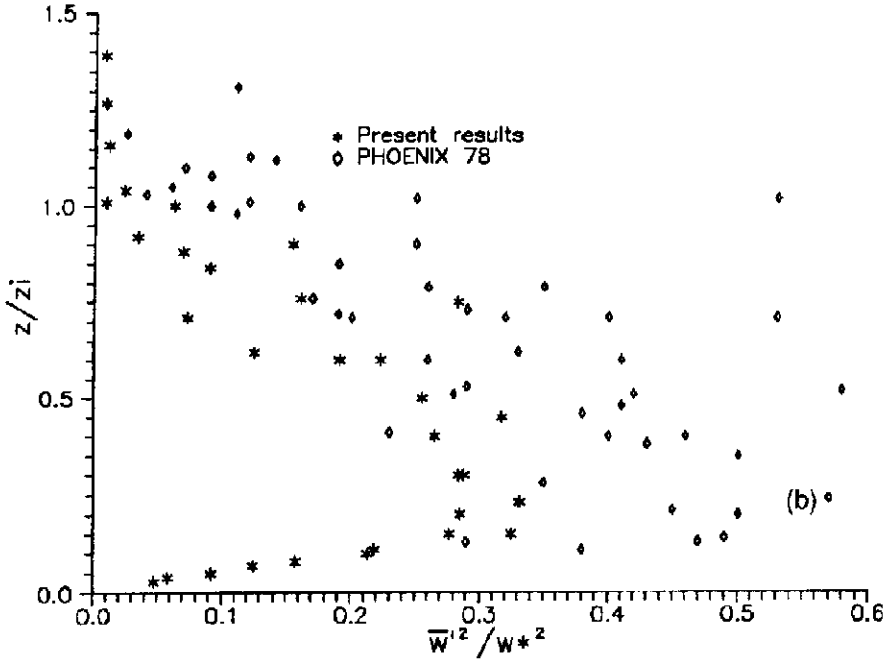

Fig. 7 - Vertical velocity variance as a function of nondimensional height. Present data are compared with Phoenix 78 (Young 1988b) field experiment.

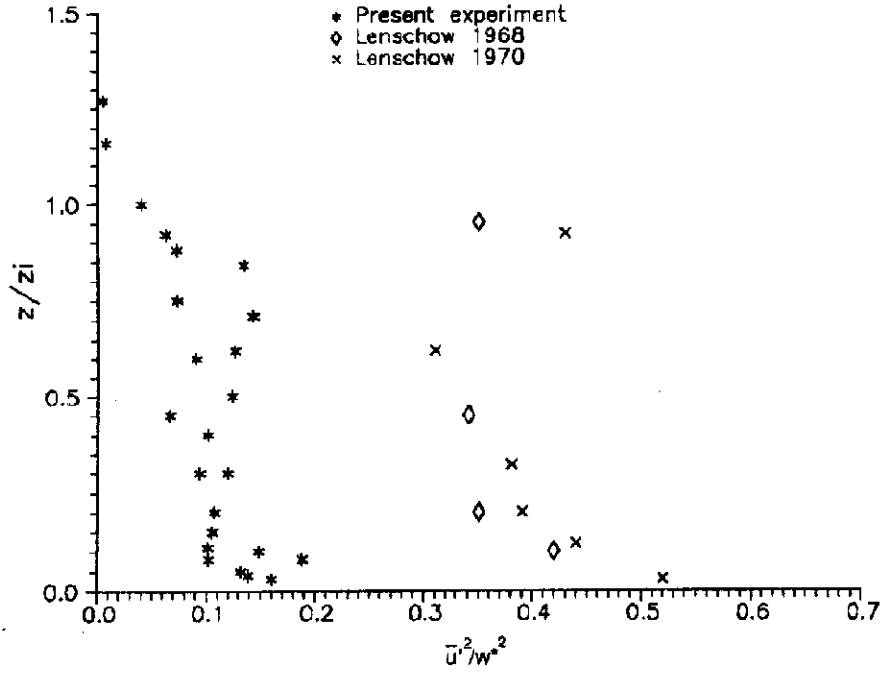

Fig. 8 - Variance of the non-dimensional horizontal velocity as a function of normalised height. Present results are compared with atmospheric experiments (After Willis and Deardorff 1974).

5.4 Probability distributions

The probability distribution of the vertical velocity, P_w, is drawn at four levels (Figure 9). P_w is defined so that $P_w\, dw/w_*$ is the probability of the occurrence of w/w_* within the $[\, w/w_* \,;\, (w+dw)/w_* \,]$ interval. The interpretation of these curves relies on the behaviour of the two main phenomena occurring in the UBL: the hot updrafts (the so called thermals)and cold downdraft (Young 1988c).

Many small updrafts arise from random locations on the lower surface, increasing in speed and merging into larger structures. They traverse the whole UBL until they are damped by the overlaying thermal stratification. Associated with these structures are the downdrafts, that slowly descend through the UBL. They have the same vertical characteristic dimension of the updrafts (order of z_i) but are broader. The typical life-time of both up and downdrafts is of order of the time for a particle to traverse the UBL, then they disappear and other similar structures take place elsewhere. Since the forcing of the convective system is the heating from below, they are not symmetrical: updrafts lead to larger ascending velocities than downdrafts, but are narrower and less probable events than the associated downdrafts.

As a consequence, the most probable value of the vertical velocity is at any height slightly negative, while the high positive velocities (due to updrafts) are characterised by low proba-

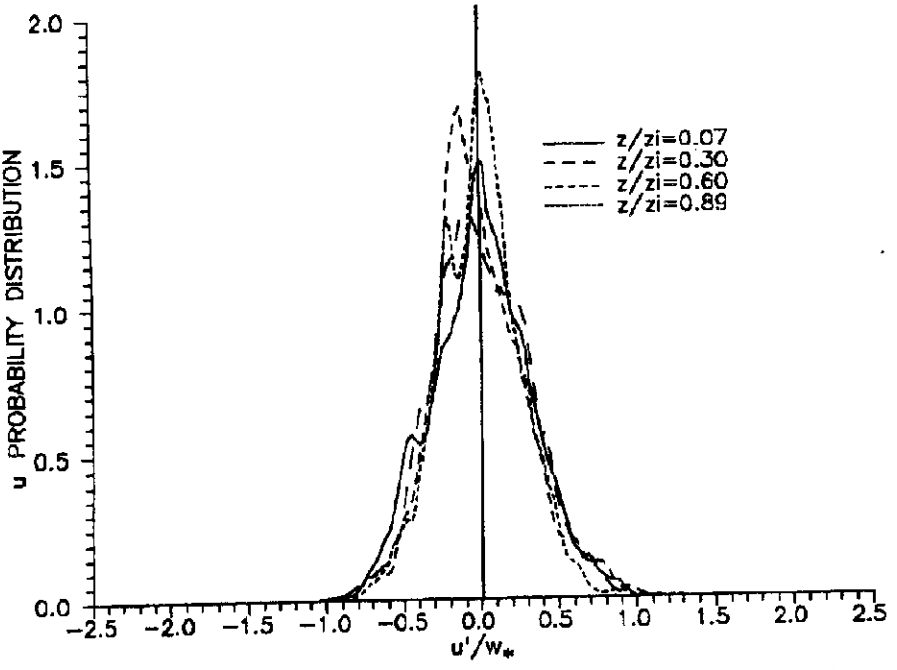

Fig. 9 - Vertical velocity probability distribution versus dimensionless velocity fluctuation at four different levels.

bility values. This asymmetry is more pronounced in the lower part of the layer, close to the thermal forcing, while the distributions tend to became symmetrical as the height increase. Conversely, the probability distribution of the horizontal velocity (Figure 10), is almost symmetric as the system does not depend on the orientation of the horizontal axis.

5.5 Joint probability

The evidence of the different behaviour of up and downdrafts is given by the joint probability function. The contour plots of the joint probability distribution of the vertical velocity component and temperature fluctuations are presented in Figure 11 for 3 levels. The distributions exhibit a maximum on the third quadrant, where velocity and temperature fluctuations are negative (cold downdraft). This supports the fact that the downdrafts are the most probable phenomenon occurring in the UBL, especially in proximity of the surface where the joint probability peak is higher than at the other levels.

Conversely, the probability distribution of the horizontal velocity (Figure 10) is almost symmetric as the system does not depend on the orientation of the horizontal axis.

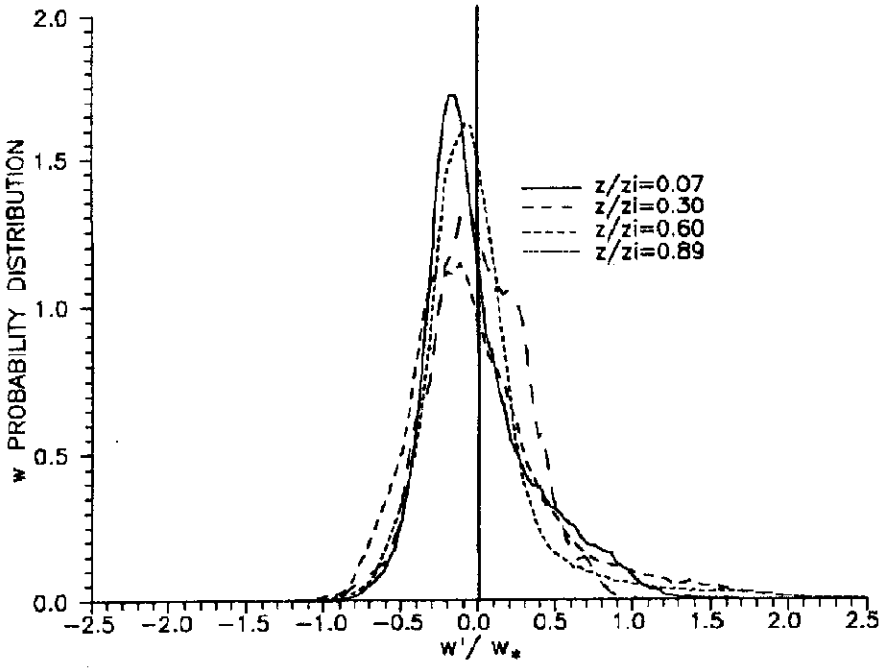

Fig. 10 - Probability distribution of the horizontal velocity at four levels.

5.6 Eulerian and Lagrangian time scales

The above discussion deals with the turbulence indicated by variations of velocity with time, as measured by an instrument probing at a fixed location. As a consequence, measurements refer to a continuously changing sample of air. This is almost the only type of measurement actually available, and it is the approach that, both experimentally and theoretically is used for the description of phenomena like the pollutant dispersion. However, it is intuitive that the diffusion of a cloud of pollutant depends on the development with time of the turbulence involving every cloud parcel (Lumley and Panofsky 1964, Monin and Yaglom 1971). In other terms, it is interesting to describe the velocity fluctuations following the motion of each air parcel, i.e. in the Lagrangian reference frame.

The direct observation of non-buoyant tracers under the action of the atmospheric turbulence is considerably difficult. Some attempts have been made in that sense (Hanna 1981). The main goal of the investigators was to find a relation between the Eulerian and Lagrangian time scales, so that, through the Eulerian measurements, the Lagrangian statistics could be determined too, but they only could suggest a value of the time scales for the bulk of the layer. From the theoretical point of view, useful results have been achieved only at the expense of intuitive hypothesis and broad assumptions (Corrsin 1963).

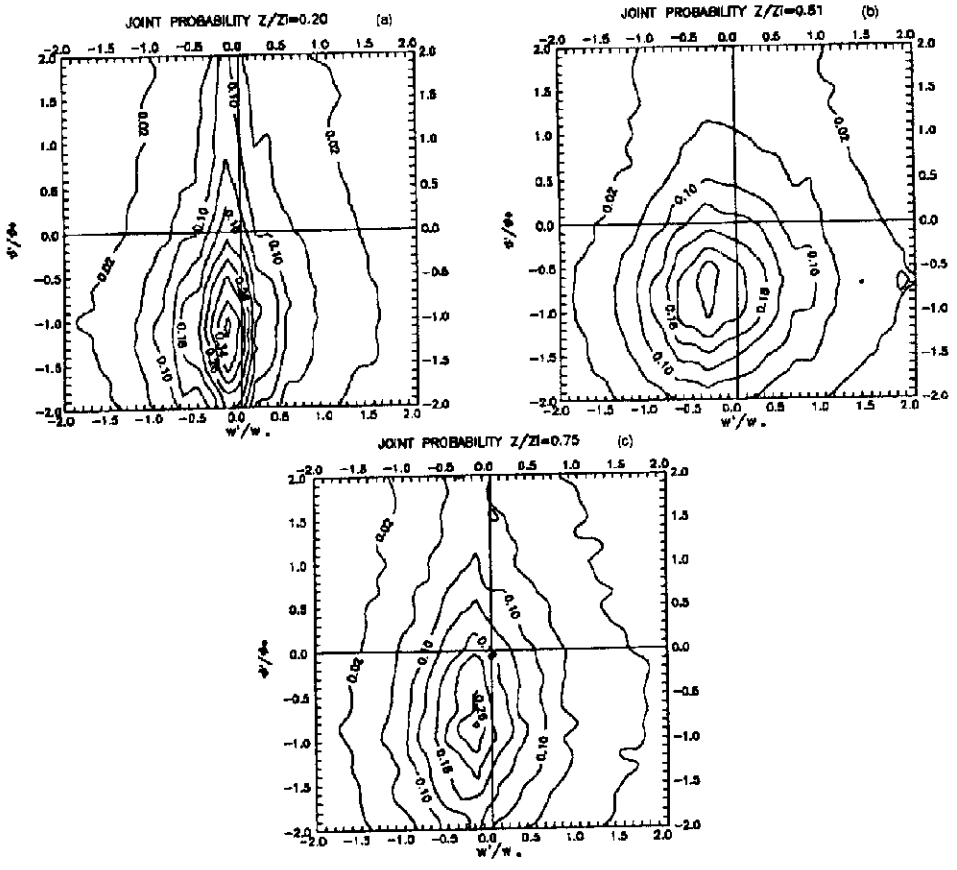

Fig. 11 - Joint probability of non-dimensional vertical velocity fluctuations and non-dimensional temperature fluctuations at the heights: $z/z_i = 0.20$ *(a);* $z/z_i = 0.51$ *(b);* $z/z_i = 0.75$ *(c).*

The PTV allows to directly obtain a Lagrangian description of turbulence, thus the Lagrangian statistics could be evaluated and compared with the Eulerian ones.
The Lagrangian integral time scale is obtained by the integration of the autocorrelation coefficient of the velocity:

$$T_L = \int_0^{\infty} R_L(\tau)\, d\tau \tag{7}$$

similarly, the Eulerian integral time scale is:

$$T_E = \int_0^\infty R_E(\tau)\, d\tau \tag{8}$$

Actually, these definitions are not suitable for experimentally determined autocorrelation functions because they do not approach to zero at the larger available time lag. So the integral time scales are obtained from the autocorrelation coefficient by estimating the time lag at which it drops to $1/e$. This is called $1/e$ scale and coincides with the former when the autocorrelation decrease exponentially $R(t) = e^{-t/T}$. Examples of Lagrangian and Eulerian autocorrelation coefficients are shown respectively in Figure 12 and 13. The Lagrangian vertical velocity is anti-correlated for time lags of about 1÷1.5 because, after that time, a fluid particle is forced to change velocity orientation at the upper or lower boundary.
In Figure 14, the integral time scales of the horizontal velocity, relative to the convective time t_*, are plotted as functions of non-dimensional height. The Lagrangian scale is large close to the top and bottom of the layer, where the main motion is horizontal, and it decreases toward the centre. The behaviour of the Eulerian scale is quite different. The reason is that the Eulerian scale is affected only by the turbulence occurring at the location where it is evaluate, while the Lagrangian one depends on the whole structure of the layer as it is evaluated from the statistics of all particles starting from a given height, wherever they go during a certain time lag. Thus the Eulerian scale is small within the Capping Inversion ($z/z_i \geq 1$), where the thermal stability damps the large scale motion, then it is almost constant in the bulk of UBL, due to the strong convective mixing, and slightly increases in the neighbourhood of the lower surface.
Figure 15 shows the integral time scales of the vertical velocity, relative to t_*, as functions of the non-dimensional height. As for the horizontal velocity, the Eulerian scale is small in the Capping Inversion and almost constant in the middle part of the UBL. Then it decreases in the zone where the turbulence is affected by the lower surface that cuts off the larger vertical structures. The Lagrangian scale is seen to continuously increase from the bottom to the top of the UBL, then it drops to small values in the Capping Inversion. The rate of growth is well approximated by the power two law:

$$\frac{T_L}{t_*} = 0.42 - 0.95\frac{z}{z_i} + 1.81\left(\frac{z}{z_i}\right)^2. \tag{9}$$

The Lagrangian time scale increases with the distance from the lower surface because, when a fluid particle reaches the surface must change velocity orientation, so it looses vertical correlation: the longer it takes to reach that boundary, the larger the Lagrangian time scale is.

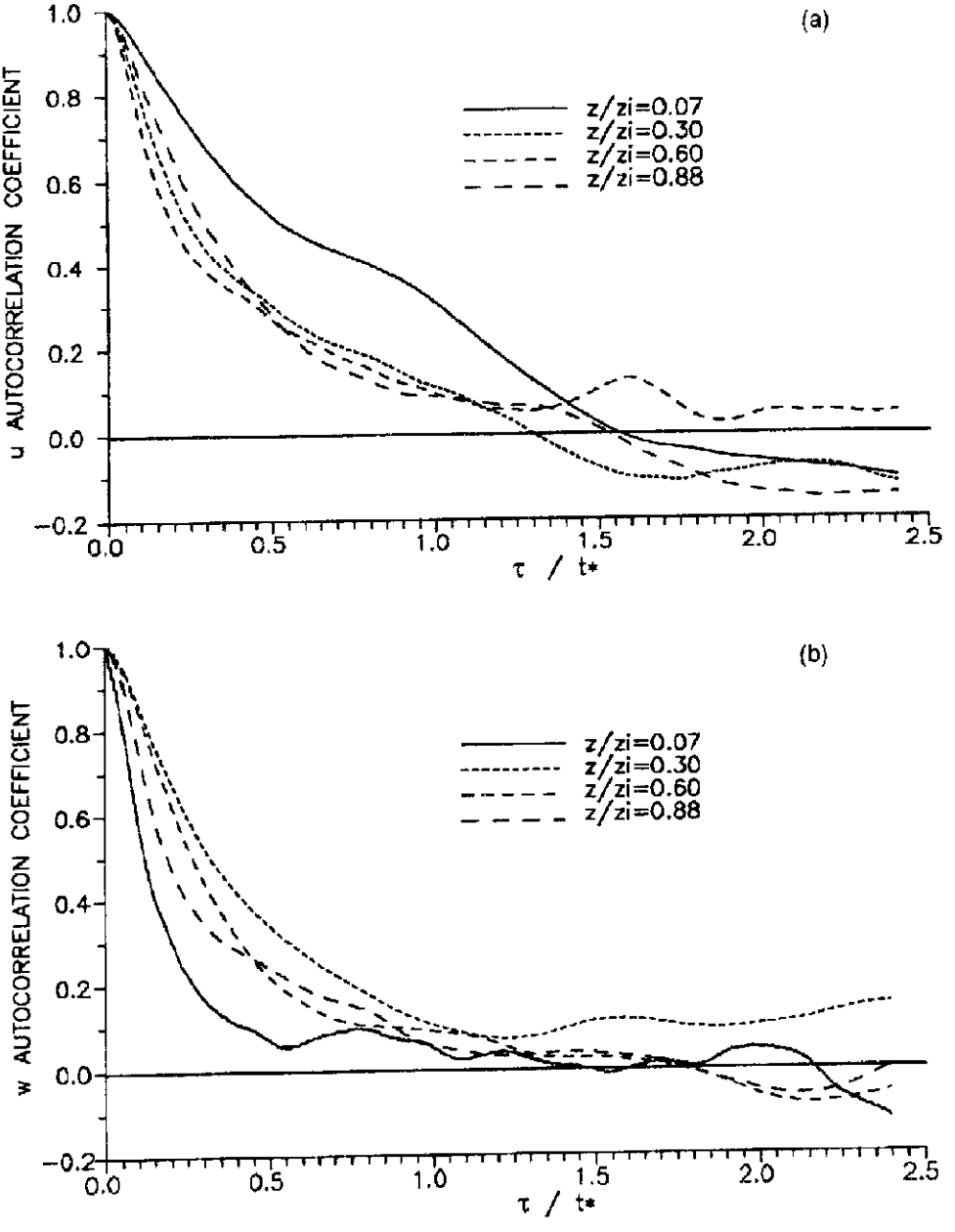

Fig. 12 - Autocorrelation coefficient of the Eulerian vertical (a) and horizontal (b) velocity versus non-dimensional time lag.

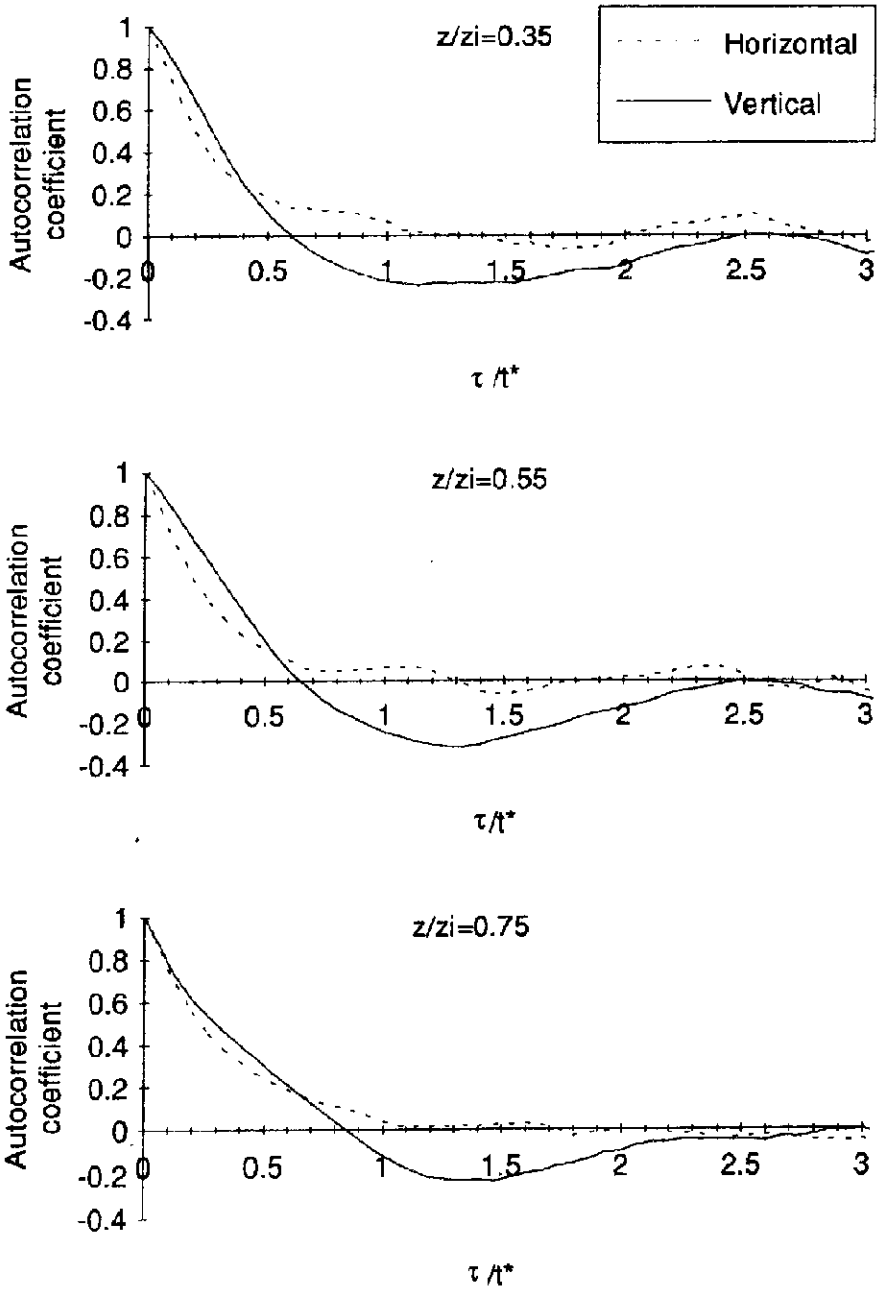

Fig. 13 - Lagrangian autocorrelation of the horizontal (dashed lines) and vertical (solid lines) components of velocity at three different levels ($z/z_i = 0.35, 0.55, 0.75$).

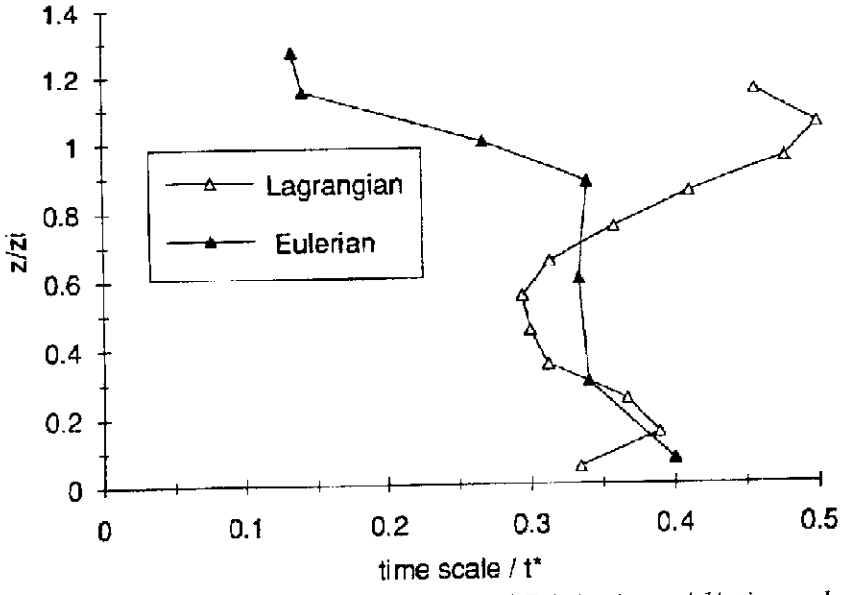

Fig. 14 - Non-dimensional profiles of the Lagrangian and Eulerian integral 1/e time scales of the horizontal velocity component.

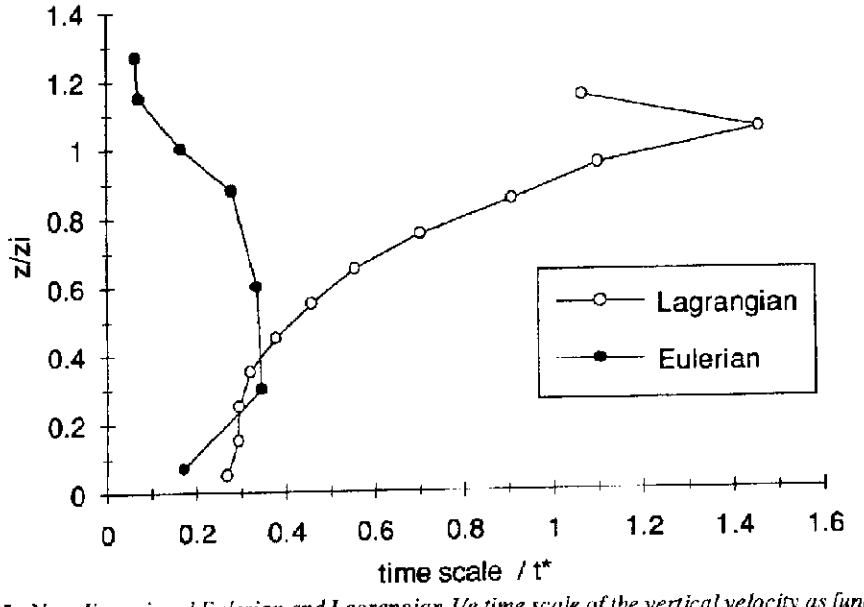

Fig. 15 - Non-dimensional Eulerian and Lagrangian 1/e time scale of the vertical velocity as functions of non-dimensional height.

5.7 Conditional time scales

In the above Lagrangian statistics, two fluid particles starting from the same height, the one related to a hot updraft and the other to a cold downdraft, give their contribution to the same term of the time scale, though their behaviour is very different. Assuming, for instance, that both particles start close to the lower surface, the uprising particle typically traverse the whole UBL and has a large time scale, while the moving-down particle takes a short time to approach the surface and loose correlation.

In order to separately describe these two phenomena, the set of trajectories acquired by the PTV, are parted into two sub-sets: the set of trajectories whose first vertical velocity is positive and the set including trajectories with negative vertical initial velocity. From these sets, the autocorrelations were evaluated and the time scales determined by means of the same techniques as above.

Figure 16 shows the upward and downward time scales of the horizontal velocity, normalised by the parameter t_*. The largest scale of the downward moving particles is observed close to the top of the layer because, in that region, the flow is slow and particles are not affected by the presence of boundary surfaces until they reach the tank bottom. A second relative maximum is located at the first third of the layer because, as above mentioned, the main motion is

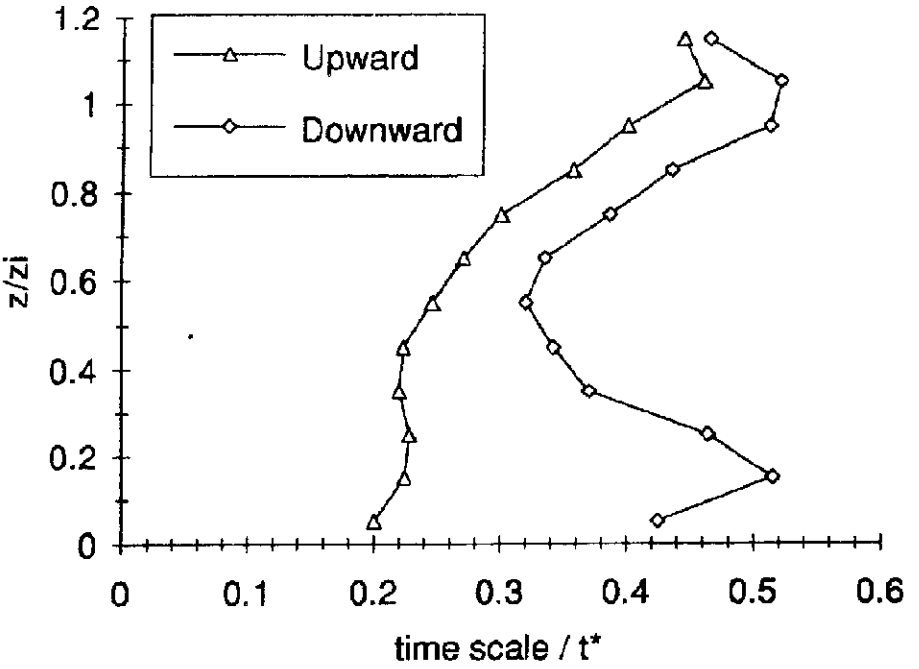

Fig. 16 - Vertical profile of the conditional Lagrangian time scales of the horizontal velocity. Triangles indicate the time scale of the trajectories whose first velocity is upwards, parallelograms indicate time scale of trajectories with negative initial vertical velocity.

horizontal. The decreased values of the time scale of the uprising particles depend on the higher velocities related to the updrafts that take less time to traverse the height of the UBL.
This is also true for the vertical velocity scales (Figure 17) that show smaller values for the uprising particles. Furthermore, the time scale of the upward moving particles decrease with height, as the starting location of particles gets closer to the upper boundary. The opposite happens for the down moving particles except for the neighbourhood of the Capping Inversion, where the scale drops because the thermal stability causes short time vertical oscillations.

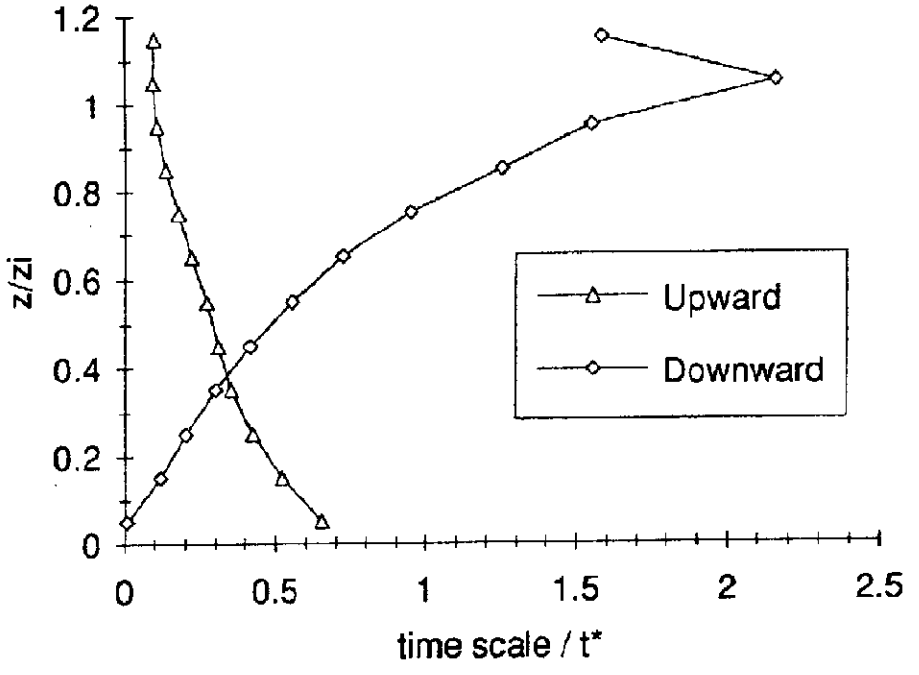

Fig. 17 - Vertical profile of the conditional Lagrangian time scales of the vertical velocity. Triangles indicate the time scale of the trajectories whose first velocity is upwards, parallelograms indicate time scale of trajectories with negative initial vertical velocity.

Conclusions

Evidence has been presented in support to the conclusion that the laboratory model well simulates the structure of the turbulence in the Unstable Boundary Layer of the atmosphere. The non-intrusive techniques used for the measurement of the velocity field allowed a detailed description of turbulence without introducing any perturbation. Furthermore, the Particle Tracking Velocimetry gave a Lagrangian description of the turbulence with an accuracy never achieved in the field experiments.
Therefore, Eulerian and Lagrangian integral time scales could be compared to outline their

vertical variability. It have been observed that, as the field is neither homogeneous nor isotropic, it is not possible to identify a single value of the Lagrangian time scales, representative of the whole Unstable Boundary Layer, though the Eulerian ones are almost constant in its middle part. Finally, by means of the conditional sampling the characteristics of the predominant phenomena of the convective mixing have been outlined.

This work has been supported by Italian Department of University and Scientific and Technologic Research (MURST).

References

Baerentsen J.H., and Berkowicz R.: 1984, 'Monte Carlo simulation of plume dispersion in the convective boundary layer', Atmos. Environ., 18, 701-712.

Corrsin S.: 1963, 'Estimates of the relation retween Eulerian and Lagrangian scales in the large Reynolds number turbulence', J. Atm. Sci., 20, 115-119.

Coulman C.E.: 1978, 'Boundary layer evolution and nocturnal inversion dispersal', Part II, Bound.-Layer Meteor., 14, 493-513.

Deardorff J.W.: 1970, 'Convective velocity and temperature scales for the unstable planetary boundary layer and for Rayleigh convection', J. Atmos. Sci., 27, 1211-1213.

Hanna S.R.: 1981, 'Lagrangian and Eulerian timescale relations in the day-time boundary layer', J. Applied Met., 20, 242-249.

Hildebrand P.H., and Ackerman B.: 1984, 'Urban effects on the convective boundary layer', J. Atmos. Sci. 41, 76-91.

Jenson L., Menon R.K., and Fingerson L.M.: 1988, 'An automatic signal processor for LDV systems', Fourth International Symposium on Applications of LASER Anemometry to Fluid Mechanics. Lisbon.

Kaimal J.C., Wyngaard J.C., Haughen D.A., Coté O.R., Izumi Y., Caughey S.J., and Readings C.J.: 1976, 'Turbulence structure in the convective boundary layer', J. Atmos. Sci., 41, 76-91.

Lenschow D.H., and Wyngaard J.C., Pennel W.T.: 1980, 'Mean-field and second moment budgets in a baroclinic, convective boundary layer', J. Atmos. Sci., 31,465-464.

Lenschow D.H.: 1974, 'Model of the height variation of the turbulence kinetic energy budget in the unstable planetary boundary layer', J. Atmos. Sci., 31, 465-474.

Lumley L., and Panofsky H.A.: 1964, 'The structure of atmospheric turbulence', Wiley, 239pp.

Monin A.S. and Yaglom A.M.: 1971, 'Statistical fluid mechanics', 2 vols., The MIT Press, Cambridge.

Stull R.B.: 1988, 'An introduction to Boundary Layer Meteorology', Kluwer Academic Publishers, pp.666.

Willis G.E., and Deardorff J.W.: 1974, 'A laboratory model of the unstable planetary boundary layer', J. Atmos. Sci., 31, 1297-1307.

Willis G.E., and Deardorff J.W.: 1976, 'A laboratory model of diffusion into the convective planetary boundary layer', Quart. J. R. Met. Soc., 102, 427-445.

Wyngaard J.C.: 1985, 'Structure of the planetary boundary layer and implications for its modelling', J. Climate Appl. Meteorol., 41, 1959-1969.

Young G.S.: 1988a, 'Convection in the Atmospheric boundary layer', Earth. Sci. Rev., 25, 179-198.

Young G.S.: 1988b, 'Turbulence structure of the convective boundary layer. Part I: Variability of normalized turbulence statistics', J. Atmos. Sci., 45, 720-726.

Young G.S.: 1988c, 'Turbulence structure of the convective boundary layer. Part II: Phoenix aircraft observations of thermals and their environment', J. Atmos. Sci., 45, 727-735.

Young G.S.: 1988d, 'Turbulence structure of the convective boundary layer. Part III: The vertical velocity budget of thermals and their environment', J. Atmos. Sci., 45, 2039-2049.